Journal of South American Earth Sciences 50 (2014) 12–26

Contents lists available at ScienceDirect

Journal of South American Earth Sciences

journal homepage: www.elsevier.com/locate/jsames

A paleomagnetic and magnetic fabric study of the Illapel Plutonic Complex, Coastal Range, central Chile: Implications for emplacement mechanism and regional tectonic evolution during the mid-Cretaceous

Rodolfo Ferrando [a,d], Pierrick Roperch [b,*], Diego Morata [a,c], César Arriagada [a,c], Gilles Ruffet [b], Maria Loreto Córdova [a,d]

[a] Departamento de Geología, Facultad de Ciencias Físicas y Matemáticas, Universidad de Chile, Plaza Ercilla 803, Santiago, Chile
[b] Géosciences Rennes, UMR CNRS 6118, Université de Rennes1, 35042 Rennes Cedex, France
[c] Centro de Excelencia en Geotermia de los Andes (CEGA), Fondap-Conicyt, Chile
[d] Servicio Nacional de Geología y Minería (SERNAGEOMIN), Santiago, Chile

ARTICLE INFO

Article history:
Received 25 April 2013
Accepted 20 November 2013

Keywords:
Paleomagnetism
Tectonic evolution
Lower Cretaceous
Coastal Range
Central Chile

ABSTRACT

The Illapel Plutonic Complex (IPC), located in the Coastal Range of central Chile (31°–33° S), is composed of different lithologies, ranging from gabbros to trondhjemites, including diorites, tonalites and granodiorites. U/Pb geochronological data shows that the IPC was amalgamated from, at least, four different magmatic pulses between 117 and 90 Ma (Lower to mid-Cretaceous). We present new paleomagnetic results including Anisotropy of Magnetic Susceptibility (AMS) from 62 sites in the plutonic rocks, 10 sites in country rocks and 7 sites in a mafic dyke swarm intruding the plutonic rocks.

Remanent magnetizations carried by pyrrhotite in deformed country rock sediments nearby the intrusive rocks indicate that tilting of the sedimentary rocks occurred prior or during the intrusion. The paleomagnetic study shows no evidence for either a measurable tilt of the IPC or a significant rotation of the forearc at this latitude range. Moreover, new $^{40}Ar/^{39}Ar$ ages exclude any medium- to low-temperature post-magmatic recrystallization/deformation event in the studied samples. AMS data show a magnetic foliation that is often sub-vertical. Despite an apparent N–S elongated shape of the IPC, the large variations in the orientation of the AMS foliation suggests that this plutonic complex could be made of several units distributed in a N–S trend rather than N–S elongated bodies.

Previous works have suggested for this area a major shift on tectonic evolution from highly extensional during Lower Cretaceous to a period around 100 Ma, associated with exhumation and compressive deformation to conform the present day Coastal Range. The low degree of anisotropy and the lack of evidence for a tectonic fabric in the intrusive rocks indicate that the shift from extensional to compressional should postdate the emplacement of the IPC, i.e. is younger than 90Ma.

1. Introduction

An intense magmatic activity (volcanism and plutonism) dominates during the Early Cretaceous evolution in the active Pacific margin of north-central and central Chile (25°20′ to 35°40′ S) (Vergara et al., 1995, and references herein). The combination of magmatism, together with basin formation, subsidence and final exhumation in this active continental margin during the Mesozoic, conform the present day Coastal Range. Along this margin, and as a consequence of major changes in the geodynamic regime of the Aluk subducting plate under the South American plate, the continental crust went through recurrent periods of extension and compression, mainly as the consequence of a continuous convergence of oceanic and continental plates (Mpodozis and Ramos, 1989; Ramos and Aleman, 2000; Arancibia, 2004; Parada et al., 2005a).

Different authors have previously concluded that a major change in tectonic conditions took place in the mid-Cretaceous (e.g. Cobbold et al., 2007). Somoza and Zaffarana (2008) argue that the beginning of contractional events in the Andes correlates with model-predicted westward acceleration of South America indicating that this change in Andean tectonic regime is associated to

* Corresponding author.
E-mail address: pierrick.roperch@univ-rennes1.fr (P. Roperch).

0895-9811/$ – see front matter © 2013 Elsevier Ltd. All rights reserved.
http://dx.doi.org/10.1016/j.jsames.2013.11.007

major plate reorganization at ca 95 Ma. For that same period, Arancibia (2004) described a contractional tectonic regime in central Chile (the Sistema de Falla Silla del Gobernador reverse fault); and other authors, using fission-track analyses, have described a rapid exhumation and uplift (Gana and Zentilli, 2000; Parada et al., 2001, 2005a). To the east of the Andes, in the Neuquen area, the beginning of Andean uplift can be bracketed between 98.6 Ma and 88 Ma (Tunik et al., 2010).

High volumes of magma were emplaced and erupted in the Coastal Range of central Chile during the Lower Cretaceous. Plutonism is partially coeval with a rather primitive volcanism, basin subsidence and a burial, non deformative, very low-grade metamorphism (e.g. Fuentes et al., 2005; Parada et al., 2005a; Morata et al., 2006).

Initially defined as "Illapel Super-unit" (Rivano et al., 1985), the Illapel Plutonic Complex (IPC) is a distinctive feature of the geology between 31° and 33 °S, exposed on an area bigger than 3200 km^2 and that is emplaced mainly into Jurassic igneous rocks, and Lower Cretaceous volcanic and sedimentary sequences. Small (few km^2), lithologically diverse gabbro and diorite bodies outcrop in this plutonic complex, mostly in its western margin and at the northern part. These mafic bodies could represent the more primitive basaltic magmas present during batholith formation. U/Pb radiometric ages obtained on magmatic titanite (Morata et al., 2006) and zircons (Morata et al., 2010) show different crystallization ages of, at least, four different magmatic pulses between 117 and 90 Ma.

We have undertaken a detailed paleomagnetic and AMS study of the IPC and obtained new $^{40}Ar/^{39}Ar$ ages with three main objectives: (1) to use the magnetic fabric to better understand the type of emplacement of the different magmatic pulses, (2) to determine possible rotations on vertical or horizontal axis related to the tectonic evolution of the forearc since its emplacement, and (3) to identify (or exclude) any low- to medium-T post-plutonic emplacement processes that could modify the primary (plutonic) magnetic signal.

2. Geological setting

2.1. Regional setting

The Lower Cretaceous volcanic-sedimentary formations of the Coastal Range conforms an almost continuous 1200 km N–S long (25°20′ to 35°40′ S) and narrow (30 km average) magmatic belt, with average thickness of 3–5 km. Volcanic rocks (mostly porphyritic high-K basaltic andesites and andesites, with minor rhyolites and ignimbritic rhyolites) dominate but sedimentary shallow marine intercalations (limestones and sandstones) can be abundant in some sections (e.g. Nasi and Thiele, 1982; Vergara et al., 1995). Three major geological formations have been described for this Lower Cretaceous belt at the latitude of Santiago (33–34° S) (Fig. 1). The oldest one, Lo Prado Formation (Thomas, 1958), consists of marine and continental volcaniclastic rocks, limestones and a bimodal sequence of dacitic ignimbrites and interbedded basalts, of assumed Valanginian and Hauterivian age. Overlying the Lo Prado Formation, the Veta Negra Formation (Thomas, 1958) is composed of continental plateau-like porphyritic "flow-basalts" and basaltic andesites, accompanied by feeder dykes and sills at the bottom whereas the uppermost levels consist of continental flow-breccias of basaltic andesitic composition. These basic products have a high-K calc-alkaline to shoshonitic affinity and a mantle-type isotopic signature being remarkably homogeneous in their mineralogical and chemical composition considering the huge volumes involved. Vergara et al. (1995) estimate more than 11,000 km^3 of volcanic materials erupted during the Jurassic and Early Cretaceous in central Chile, corresponding to a minimum effusion rate of

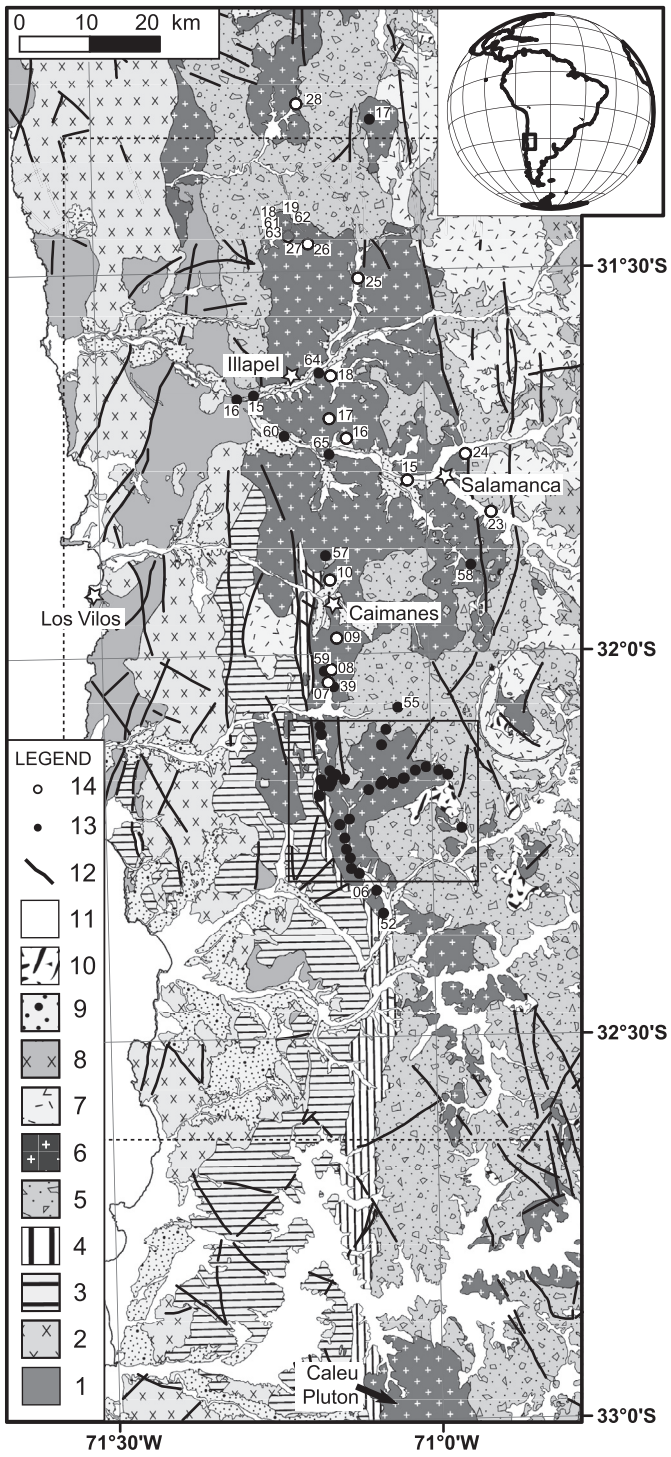

Fig. 1. Regional geological map of central Chile (31°30′-32°30′ S) modified and simplified from the 1:250,000 geological maps of Chile, Rivano and Sepúlveda (1991) and Rivano et al. (1993), showing the main units in this area. Legend: 1 = Upper Paleozoic and Triassic igneous and stratified rocks; 2 = Jurassic igneous rocks; 3 = Jurassic stratified rocks; 4 = Lo Prado Formation (Lower Creataceous); 5 = Stratified continental and volcanic rocks from Lower to middle Cretaceous; 6 = Illapel Plutonic Complex; 7 = Upper Cretaceous continental and volcanic rocks; 8 = Upper Cretaceous and K-T igneous rocks; 9 = Cenozoic volcanic and continental rocks; 10 = Rocks with strong hydrothermal alteration; 11 = Quaternary; 12 = Major tectonic lineaments; 13,14 = Paleomagnetic sites with code MR and LC respectively in data Tables. Rectangle to the south corresponds to the Las Palmas locality with more details of the sampling shown in Supplementary Fig. 1. The box delineated by dotted lines corresponds to area shown in Figs. 2 and 13.

140 km^3/Ma. ^{40}Ar/^{39}Ar dating in plagioclases from some lavas of the Veta Negra Formation (or the equivalent Arqueros Formation to the north of the study area; Morata and Aguirre, 2003) indicates a concordance of ages for the volcanism in the range 114–119 Ma (Aguirre et al., 1999; Morata et al., 2001; Fuentes et al., 2005; Morata et al., 2006). Finally, overlying this volcano-sedimentary sequence, the Las Chilcas Formation, a molasse-type formation mainly composed by sandstones, volcano-sedimentary breccias and thick strata of coarse-grained conglomerates and breccias, represents the end of the Early Cretaceous cycle in the Coastal Range. A Mid-Albian (~105 Ma) age has been deduced from marine planktonic microfossils found in limestone at the lower levels of the Las Chilcas Formation (Martínez-Pardo et al., 1994). Zircon U–Pb ages of 109.6 ± 0.1 and 106.5 ± 0.2 Ma and whole rock K–Ar ages of 101 ± 3 and 100 ± 3 Ma have been obtained by Wall et al. (1999) in felsic volcanic rocks of the lower section of this formation. Moreover, Godoy et al. (2006) reported U–Pb SHRIMP ages of 112 ± 1.2 Ma in an ignimbrite flow and 113 ± 0.8 Ma in an andesite at the ≈34°S in rocks, which could be assigned to the Las Chilcas Formation.

Closely related in space to the volcano-sedimentary belt, Cretaceous plutonic rocks, belonging to the Coastal Batholith (hornblende bearing tonalites, trondhjemites and granodiorites resembling the rocks of the TTG suites) were emplaced at low-pressure conditions (Parada et al., 1988, 1999). A magmatic gradient has been recognized in one of these plutons, the Caleu pluton, a N–S elongated composite pluton about 40 km northwest of Santiago and not far south from the IPC (Fig. 1), showing lithologies ranging from gabbro to granodiorites (Parada et al., 2002, 2005a). U–Pb zircon ages suggests an age of emplacement in the interval 94.2–97.3 Ma, with rapid subsolidus cooling between 550 and 500 °C and 250 °C as documented by the ^{40}Ar/^{39}Ar plateau ages on amphibole, biotite and plagioclase between 94.9 ± 1.8 and 93.2 ± 1.1 Ma (Parada et al., 2005a). Moreover, this is the only pluton in the Coastal Cordillera of central Chile on which a systematic paleomagnetic study has been carried out (Parada et al., 2005b).

K–Ar ages (on biotite, amphibole and/or whole-rock) are also available on other Lower Cretaceous plutons (e.g. Rivano and Sepúlveda, 1991; Rivano et al., 1993), with ages ranging from 130 to 97 Ma. All these ages suggest that plutonism and volcanism are coeval, at least in this segment of the Coastal Range.

Another general characteristic of this Lower Cretaceous belt is the systematic presence of a pervasive and non-deformative very-low to low grade metamorphism which affects the lavas. As previously described, the petrologic characteristics of this metamorphism correspond to the burial, non deformative model of very low to low-grade, essentially covering the range of the zeolite, prehnite-pumpellyite, and low-greenschist facies, i.e. with *P* and *T* values less than 3 kb and 350–400 °C respectively (Levi, 1969; Levi et al., 1982, 1989; Aguirre et al., 1989, 1999). Based on ^{40}Ar/^{39}Ar plateau ages in adularia from amygdales from basaltic flows of Veta Negra Formation, time interval between volcanism and metamorphism of about 22–25 Ma has been obtained, allowing the calculation of subsidence rate in the range 150–180 m/Ma for this Lower Cretaceous basin (Aguirre et al., 1999; Fuentes et al., 2005). The coincidence in age between plutonism and the low-grade metamorphism of the volcanic rocks suggests that this last was not solely produced by burial but also related to a regional increase in thermal gradients associated with the thermal anomaly necessary to generate the plutonism (Fuentes et al., 2005; Parada et al., 2005a). In this sense, this very low-grade metamorphism can be classified as a type of diastathermal metamorphism according to Robinson and Bevins (1989).

2.2. The Illapel Plutonic Complex

2.2.1. The plutonic rocks

The Illapel Plutonic Complex (Parada et al., 1999), early defined by Rivano et al. (1985) as Illapel Super unit, is mainly emplaced into Lower Cretaceous volcanic and sedimentary rocks (Fig. 1). Previous biotite K–Ar ages gives a range of age of 113 ± 3 Ma to 96 ± 3 Ma (Fig. 2), though new U/Pb determinations analyzed in magmatic titanites show differences in the age of crystallization of different magmatic intrusions between 105.9 ± 1.5 and 97.7 ± 0.5 Ma (Morata et al., 2006). Morata et al. (2010) defined four magmatic intrusion: a mafic unit (MU), dominantly composed of gabbro and diorite that outcrops on the northwestern part of the IPC; a trondhjemitic unit (TU) mainly composed by trondhjemite and leucogranite, and dominantly present on a N–S band at the north-central part of the IPC; a main tonalitic unit (MTU) with different proportions of mafic microgranular enclaves (MME), with different forms and sizes (Varas et al., 2009), and ages between 102.4 ± 1.5 and 98.8 ± 1.3 Ma that outcrops in a N–S band at the central and south part of the IPC; and finally, the granodioritic unit (GU), in the eastern border of the IPC, composed dominantly of granodiorites with only a sample dated by K/Ar biotite age of 85.9 ± 2.2 Ma (Fig. 2).

The IPC would have been emplaced at shallow depths of 1.6–1.7 kbar (Varas et al., 2012). On the other hand, the existence of big xenoliths of volcanic and sedimentary rocks as roof pendant would

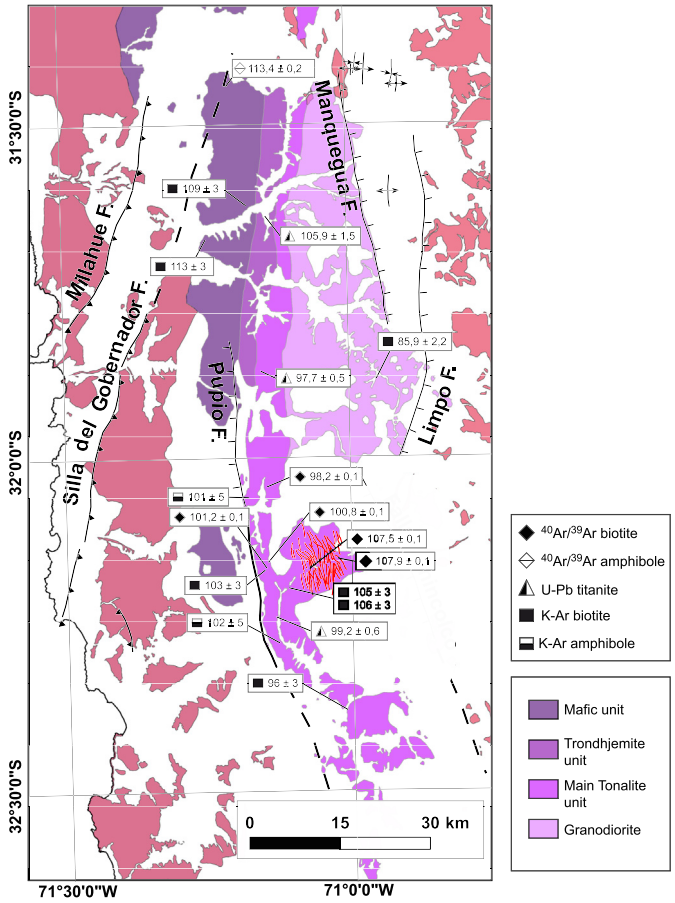

Fig. 2. Simplified IPC scheme with the distribution of U–Pb ages modified from Morata et al. (2006). ^{40}Ar/^{39}Ar ages, this study; U–Pb in titatine from Morata et al. (2006); K–Ar in biotite from Rivano et al. (1985, 1993); K–Ar in amphibole from Rivano et al. (1993).

indicate that still it is possible to observe the roof of at least one of the pulses that builds the IPC.

2.2.2. The Frutillar dike complex

A complex of mafic dikes intrudes the IPC in Quebrada Frutillar (Fig. 1, Supplementary Fig. 1). These mafic dikes, ranging in composition from basalt to basaltic andesites, have porphyritic to doleritic textures composed by clinopyroxene-plagioclase as main primary mineral. Dikes are sub-vertical with N350° to N330° orientation and present a rather pervasive low-temperature (epidote-albite-chlorite) alteration with some epidote veins significantly oblique to the dike border.

2.2.3. Mafic microgranular enclaves (MME)

Centimeter to meter sized MME, dioritic in compositions, mainly composed by amphibole, plagioclase, biotite, magnetite and quartz, were incorporated in the MTU. Thermobarometric studies based on amphibole-plagioclase composition suggest similar values for the crystallization temperature (720 ± 75 °C) under a low pressure of 1.7 ± 0.6 kbar both for MME and host-rocks (Varas et al., 2012). At some sites, we perform a comparative AMS study between the enclaves and the tonalite to test the hypothesis of a possible reset of the magmatic fabric by a late stage of deformation.

2.3. IPC host rocks

As previously described, the IPC is emplaced mainly into Lower Cretaceous volcanic and sedimentary sequences (Fig. 1), but also at a minor extent into oldest rocks. Broadly, the IPC is in contact with Lower Cretaceous porphyritic lavas sequences (Veta Negra Formation) to the east, meanwhile to the north-west, the IPC is in contact with Lower Cretaceous lavas, Triassic sandstones (El Quereo Formation) and Jurassic rocks (sedimentary and igneous) and in the south-west border with an almost N–S thin band (<5 km) of deformed limestones of the Early Cretaceous age (Lo Prado Formation). We will only describe the rocks from which we extracted paleomagnetic samples.

El Quereo Formation: It is approximately a 700 m thickness Triassic sedimentary sequence mainly composed of fine to medium coarsed sandstones, turbidites and black shales (Muñoz Cristi, 1942; Rivano and Sepúlveda, 1991). This sequence unconformably overlies different Paleozoic units, and underlies the thick silicic Pichidangui Formation of Ladinian-Carnian age (Rivano and Sepúlveda, 1991). In the study area, the sequence is composed mainly of fine to coarse sandstones with bedding tilted to the west.

Lo Prado Formation: This formation contains marine Valanginian-Hauterivian sedimentary and volcanic unit, consisting of a bathyal marine sequence covered by ignimbrites interbedded with coastal and continental sedimentary rocks (Vergara et al., 1995). Boric and Munizaga (1994) obtained a plagioclase $^{40}Ar/^{39}Ar$ plateau age of 132 Ma from a mineralized dike, and they assigned this age to the volcanism of this formation.

In the study area, this formation is mainly represented by highly deformed sedimentary rocks, in the southern border of the IPC (Fig. 1). A contact metamorphism aureole with hydrothermal alteration zones hosting mainly stratabound copper mineralization is present in the southern border of the IPC.

The **Veta Negra Formation** is a volcanic unit consisting of a thick pile of highly porphyritic plagioclase-rich basaltic andesitic and andesitic lava flows (locally known as “ocoites”), with subordinate interbedded sediments, emplaced in a continental environment. Stratigraphic relations indicate a Barremian-Albian age. Vergara and Drake (1979) dated these lava flows at 105 Ma (K/Ar in plagioclase) but more precise $^{40}Ar/^{39}Ar$ plagioclase plateau ages (Aguirre et al., 1999; Fuentes et al., 2005) constrain this magmatic event in the 119–117 Ma interval.

In the study area the Veta Negra is intruded by the IPC, but unlike what happens with the Lo Prado Formation, Veta Negra Formation is not deformed and there is no widespread contact metamorphism, although there are areas with strong hydrothermal alteration that could be related to the emplacement of the IPC.

3. New $^{40}Ar/^{39}Ar$ dating

3.1. Sampling and methodology

Seven samples were analyzed with an $^{39}Ar–^{40}Ar$ laser probe (CO_2 Synrad®). Analyses were performed on millimetric single biotite or amphibole minerals.

Minerals were carefully handpicked under a binocular microscope from crushed rocks (0.3–2 mm fraction). The samples were wrapped in Al foil to form packets (11 mm × 11 mm × 0.5 mm). These packets were stacked up to form a pile, within which packets of flux monitors were inserted every 8 to 10 samples. The stack, put in an irradiation can, was irradiated for 13.33 h (integrated power 40 MWH) at the McMaster reactor (Hamilton, Canada) with a total flux of 1.2×10^{18} n.cm^{-2}. The irradiation standard was the sanidine TCR-2 (28.34 Ma according to Renne et al., 1998). The sample arrangement allowed us to monitor the fluence gradient with a precision of ±0.2%.

Ruffet et al. (1995, 1997) describe in details the step-heating experimental procedure. Blanks are performed routinely each first or third run, and are subtracted from the subsequent sample gas fractions. Analyses are performed on a Map215® mass spectrometer.

To define a plateau age, a minimum of three consecutive steps are required, corresponding to a minimum of 70% of the total ^{39}Ar released, and the individual fraction ages should agree to within 1s or 2s with the integrated age of the plateau segment. All discussed $^{39}Ar/^{40}Ar$ results are displayed at the 1σ level (Fig. 3).

3.2. Results

The selection of samples for Ar/Ar geochronology was made to better constrain the age and the cooling history of the plutonic units defined in the IPC.

The sole analyzed amphibole (MR19) displays a slightly saddle shaped age spectrum which nevertheless allows a plateau age calculation at 113.4 ± 0.2 Ma (Fig. 3). This sample was collected from a layered gabbro located at the northern border of the IPC. As the slight observed saddle shape could express presence of some excess argon, the calculated plateau age would have to be viewed as a maximum estimate of the emplacement age of the gabbro.

Five of the six biotites analyzed display $^{40}Ar/^{39}Ar$ plateau ages ranging from 98.2 ± 0.1 Ma to 107.9 ± 0.1 Ma when biotite MR23 yields a disturbed age spectrum, characteristic of chloritization (Ruffet et al., 1991). Felsic samples MR31 and MR47 were collected in granitic and granodioritic facies, respectively. Despite some weathering observed in the field and under microscope, selected apparently unaltered biotites displayed highly concordant plateau ages at 107.9 ± 0.1 Ma and 107.5 ± 0.1 Ma (Fig. 3) respectively.

Samples MR08 and MR39 correspond to very fresh tonalites from the MTU, collected very close to the area on which Morata et al. (2010) obtained an U/Pb titanite age of 99.2 ± 0.6 Ma (Fig. 2). For both samples, biotites display rather flat age spectra with plateau ages at 100.8 ± 0.1 and 98.2 ± 0.1 Ma, consistent with U/Pb titanite age (Fig. 2).

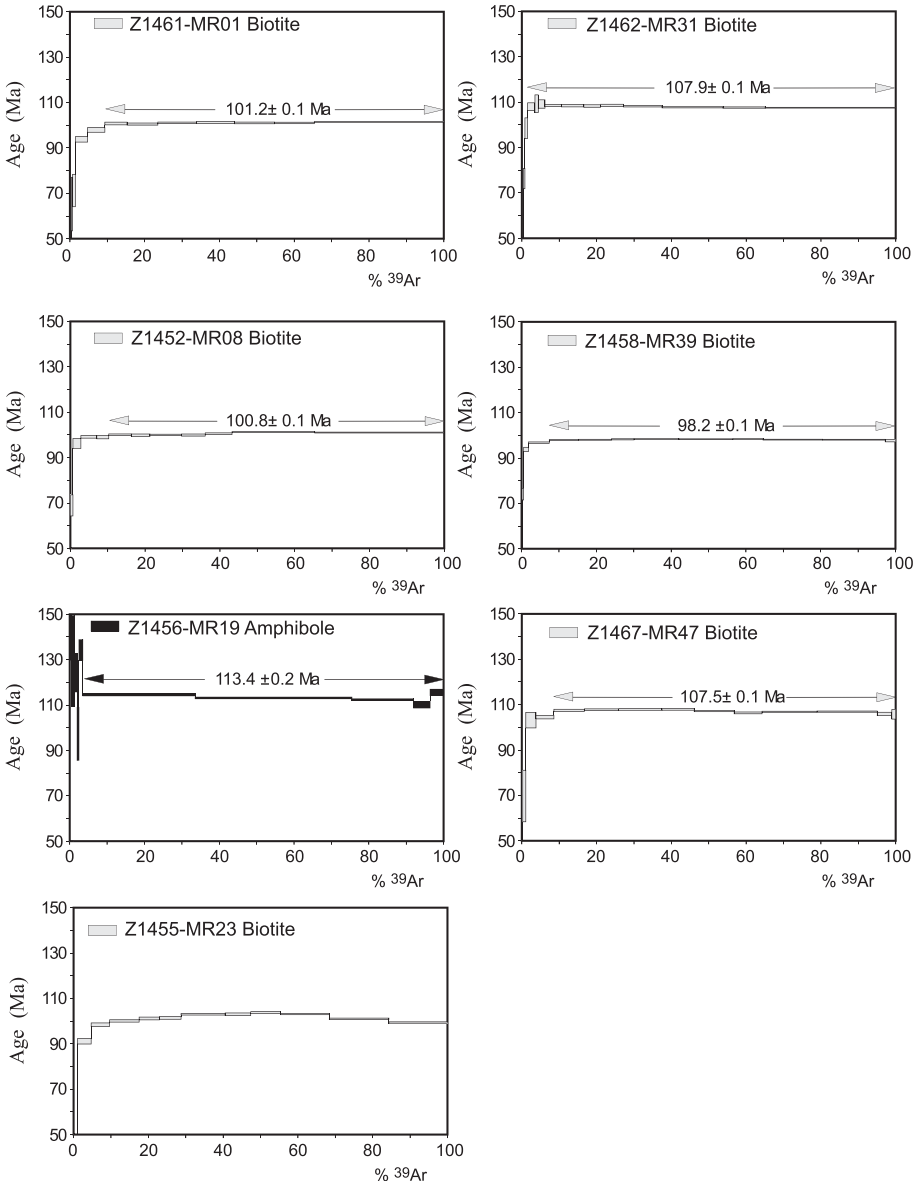

Fig. 3. $^{40}Ar/^{39}Ar$ dating of 6 samples from the IPC. The disturbed plateau-age for sample MR23 was not taken into account.

Biotite MR01 that allows characterizing the MTU yields a plateau age at 101.2 ± 0.1 Ma (Fig. 3).

4. Paleomagnetic results

4.1. Sampling and methodology

Seventy nine paleomagnetic sites (Fig. 1, Supplementary Fig. 1, and Supplementary data) were sampled with a portable drill, with about 5–8 cores per site. Sixty nine sites were taken mainly from the Illapel Plutonic Complex of which 6 sites come from the gabbro unit. Seven sites come from the dikes intruding IPC rocks in Quebrada Frutillar. In addition, 10 sites were taken from the IPC host rocks: five from sedimentary sequences and the other five in volcanic rocks. Standard paleomagnetic core samples were oriented in the field, both magnetically and with solar azimuth.

The magnetic properties of rocks were measured in the laboratory of Paleomagnetism of the Department of Geology, University of Chile (Santiago, Chile), and in the paleomagnetic laboratory at Université de Rennes1 (Rennes, France).

Natural Remanent Magnetization (NRM) was measured with a JR5 spinner magnetometer or with a cryogenic magnetometer (2G Cryogenic magnetometer with 3 axes alternating field (AF) online demagnetization). Additionally, volumetric magnetic susceptibility was measured from the same specimens with a Bartington MS2 susceptibility meter. The samples were demagnetized by AF or thermally with the ASC Scientific TD48 thermal demagnetizer. Isothermal remanent magnetization (IRM) were given with an ASC Scientific pulse magnetizer.

The low-field anisotropy of magnetic susceptibility (AMS) is a rapid and non destructive method to estimate rock fabrics (see Borradaile and Henry, 1997 for a review of the AMS technique). AMS was measured on one or two specimens per core with an Agico Kappabridge (KLY3-S). Anisotropy of anhysteretic remanent magnetization (AARM) was determined on few specimens to compare with the AMS. AARM was given under a dc field of less than 100 μT. Since the degree of AARM tends to increase with lower coercivity and larger grain size (Astudillo et al., 2005), we used low AF fields < 50 mT to enhance the AARM.

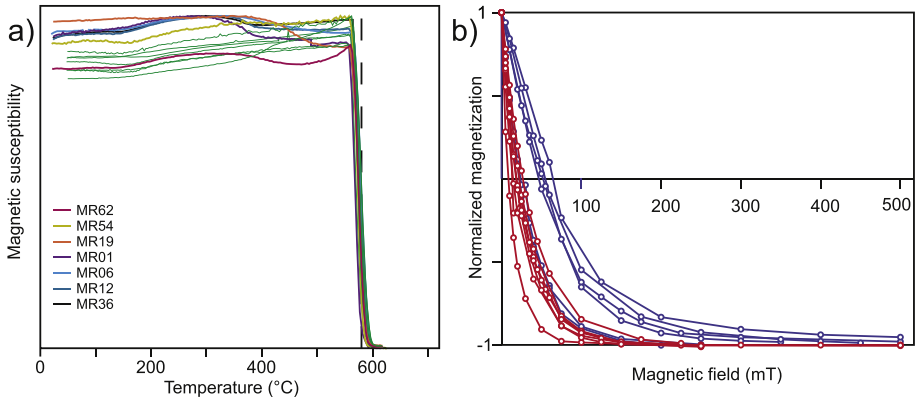

Fig. 4. a) Magnetic susceptibility versus temperature curves for seven IPC samples showing Curie points of 580 °C typical of the one of magnetite shown by the dashed line. The heating curves are shown in color with a color code corresponding to the sample number. All cooling curves are shown in green. b) Backfield Isothermal remanent magnetizations for IPC samples with respectively low (red curves) and high magnetic stability (blue curves) during thermal or AF demagnetizations.

4.2. Magnetic properties and characteristic directions

4.2.1. The IPC intrusive rocks

Most samples, except those obtained in trondjhemite, have high magnetic susceptibility (>0.01 SI). Samples from the gabbros have the highest magnetic susceptibility (>0.1 SI). The main magnetic mineral is magnetite with Curie temperature around 580 °C (Fig. 4a). IRM experiments show that saturation is acquired below 250 mT and often below 150 mT for samples of the MTU with remanent coercivity in the range 10–20 mT (Fig. 4b).

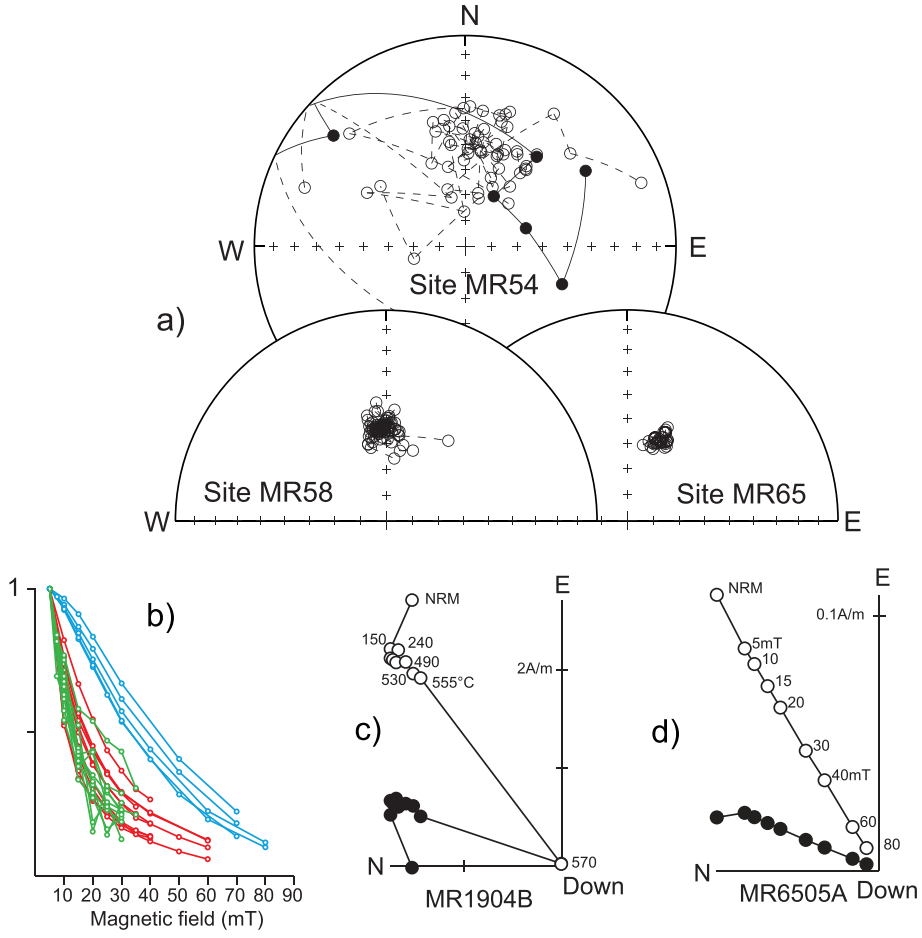

Fig. 5. a) Equal-area projection of the paleomagnetic directions (open circles for negative inclinations) during the AF demagnetization for all samples from three sites. Site MR65 (trondjhemite facies) and MR58 correspond to IPC rocks with respectively very good and good magnetic stability and for which characteristic directions were easily determined. Site MR54 is a typical site from the tonalite facies for which it has not been possible to determine well-defined characteristic directions. b) Normalized variation of the intensity of the remanent magnetization versus intensity of the applied AF field (mT) for samples of sites MR65 (blue curves), MR58 (red curves) and MR54 (green curves). Orthogonal projections (in situ) of thermal (c) and alternating field (d) demagnetization data of two IPC samples (from sites MR19 and MR65). Solid (open) circles correspond to projection into the horizontal (vertical) plane.

The intensity of the remanent magnetization is relatively low for samples from the MTU (<0.2 Am^{-1} in most cases). These samples have low medium destructive fields (MDF) upon AF demagnetization (5–10 mT) and it was not possible to determine well-defined characteristic directions for most sites of this unit (Fig. 5a). The thermomagnetic data and the low remanent coercivity observed in IRM acquisition indicate that multidomain magnetite is the magnetic carrier in the MTU.

In contrast, despite the high magnetic susceptibility, samples from the gabbros have stable remanent magnetizations with MDF values in between 20 and 50 mT and a narrow unblocking temperature range (550–580 °C) during thermal demagnetization (Fig. 5c). Fine-grained titanomagnetite inclusions in pyroxenes and plagioclases often explain the good stability of the remanent magnetization in mafic intrusive (Feinberg et al., 2005 and references herein).

Trondjhemitic rocks have low magnetic susceptibility and high MDF values (>50 mT). These samples have the most stable remanent magnetizations either upon AF or thermal demagnetization (for example site MR65, Fig. 5a,d).

In agreement with the late Early Cretaceous age, all the characteristic directions are of normal polarity. Except the two most northern sites LC28 and MR17 (sampled north away from the main IPC outcrops, Fig. 1) showing a clockwise rotated declination, all sites are well grouped. Although the gabbro unit is slightly older, the mean direction calculated for this group of sites is not different from the means calculated for the other groups of sites in younger IPC units (Fig. 6).

4.2.2. The Frutillar dyke complex

The magnetic property of the seven dikes is variable. Five dikes have high magnetic susceptibility while two dikes (MR48, MR49) have low magnetic susceptibility (Supplementary data and Supplementary Fig. 2). Thermal demagnetization of samples from the mafic dikes indicate two magnetic carriers, one with unblocking temperature range of 150–300 °C and a second with

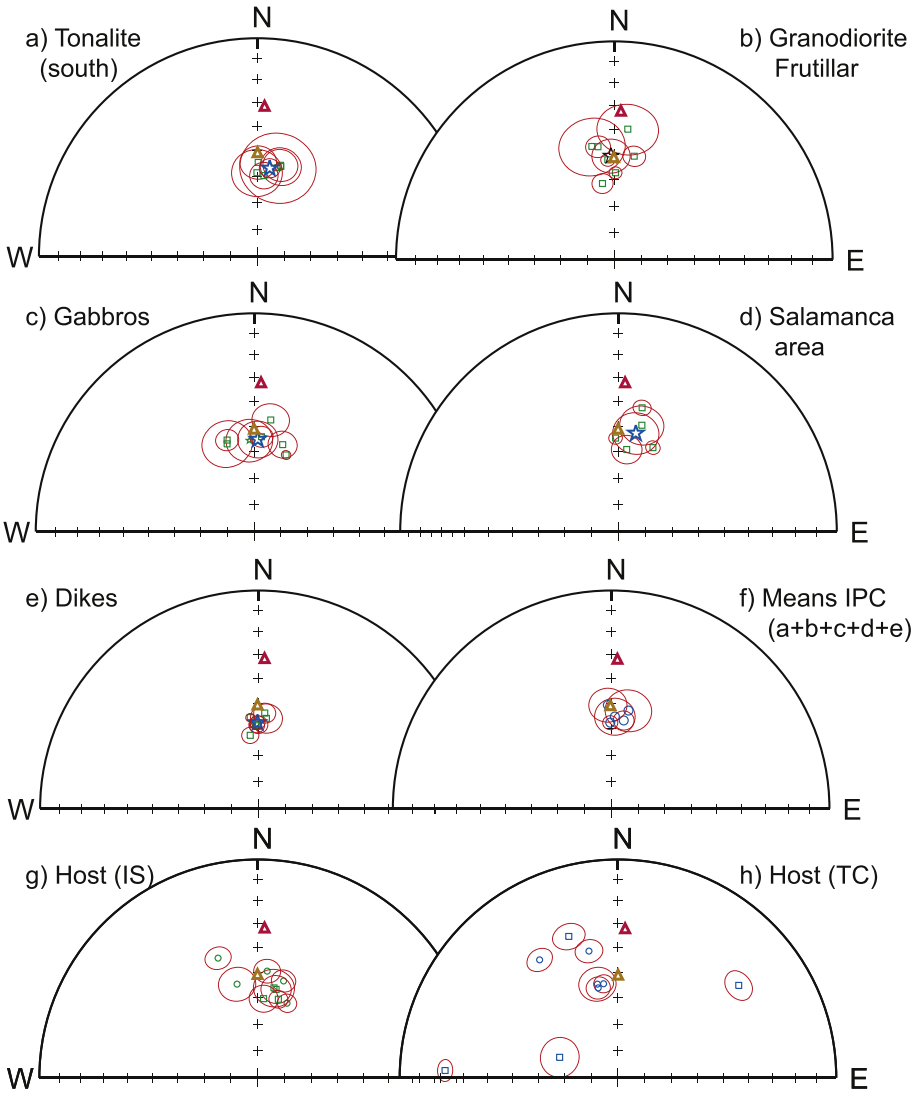

Fig. 6. Equal-area projection of the site-mean characteristic directions (green squares) with 95% confidence angles (red circles). The mean for the group of sites is shown with a blue star. a) Results from the tonalites near the Las Palmas localities; b) sites in granodiorite (Frutillar area); c) sites from the northern gabbro (MU); d) other sites from the MTU north of the Las Palmas locality; e) sites from the dike swarm; f) plots of the five locality-mean directions; g & h) site-mean directions in the IPC host rocks in situ and after tilt correction respectively. The squares correspond to the sedimentary host rock sites and circles are the volcanic host rock sites. The red and orange triangles correspond to the present-day field direction and the dipolar field direction respectively. Open (filled) circles (squares) are projection in the upper (lower) hemisphere and correspond to negative (positive) inclinations.

unblocking temperatures above 500 °C. However, the direction of the magnetization in the low unblocking temperature range (150–300 °C) is the same than the direction carried by magnetite with unblocking temperatures above 300 °C (Fig. 7b). Titanomagnetite is likely the main magnetic carrier for the low temperature component (Fig. 7b). The decrease in the magnetic susceptibility measured at room temperature after each heating step and thermomagnetic experiments (Fig. 7a) indicates that the titanomagnetite is slightly altered to titanomaghemite. This alteration is consistent with the low-temperature alteration mineralogy also observed in these dikes. Dikes with low magnetic susceptibility have also stable univectorial magnetization but with higher unblocking temperatures carried by magnetite without evidence of maghemitization (Fig. 7c).

The characteristic directions determined for the 7 dikes are highly grouped providing a mean-direction with the lowest angle of confidence at 95% that is not statistically different from the mean calculated from the 25 sites taken from the plutonic units (Fig 6e).

4.2.3. IPC host rocks

Paleomagnetic sites taken from the host rocks of the IPC come mainly from the Las Palmas locality in the southern part of the study area (see Supplementary Fig. 1). In this area, the western border of the IPC is in contact with limestones from the Lo Prado Formation. These limestones are hardly deformed and strongly recrystalized as a consequence of intrusion, with a contact metamorphic aureole over hundreds of meters from the edge of the igneous body.

During the thermal demagnetization of these limestones, most samples present a characteristic component with unblocking temperatures below 320 °C (Fig. 7e). Curie point of 320 °C (Fig. 7d) is in agreement with pyrrhotite being the magnetic carrier (approximately 325 °C; Dekkers et al., 1989).

At the Illapel latitude (Fig. 1), we have sampled one approximately 10 m thick recrystalized sedimentary sequence (site MR16) from the Triassic El Quereo Formation, taken at the western edge of the IPC. This sequence is mainly composed by fine to coarse sandstones and oriented N5°W/55°W approx. Unblocking temperatures indicate also that pyrrhotite is the main carrier (Fig. 7f). The large scatter upon tilt correction (see Fig. 6 g–h) demonstrates that the magnetization was acquired after tilting and the formation of pyrrhotite indicates that the remagnetization is likely associated with contact metamorphism during the IPC intrusion.

Towards its eastern edge, the IPC is in contact with the Veta Negra and Las Chilcas formations (Fig. 1), although the latter appears to be with a normal fault contact at Salamanca locality (Rivano and Sepúlveda, 1991). The remanent magnetization of samples from the volcanic flows is of variable intensity. While site MR28 presents a high intensity and stable remanent magnetization carried by magnetite, site MR29, consisting of a strongly altered rock with low magnetic susceptibility, has a NRM of low intensity but with a very stable and univectorial magnetization. The altered nature of the rock at site MR29 suggest a secondary magnetization but site MR28 likely records a primary magnetization. The low bedding correction impedes a clear tilt correction test to check for a possible remagnetization of the volcanic rocks by the IPC (Table 1).

5. Magnetic fabric

5.1. The gabbro unit

Although all the sites in the gabbros were sampled very closely (Fig. 1), the changes in the magnetic fabric in directions and shape

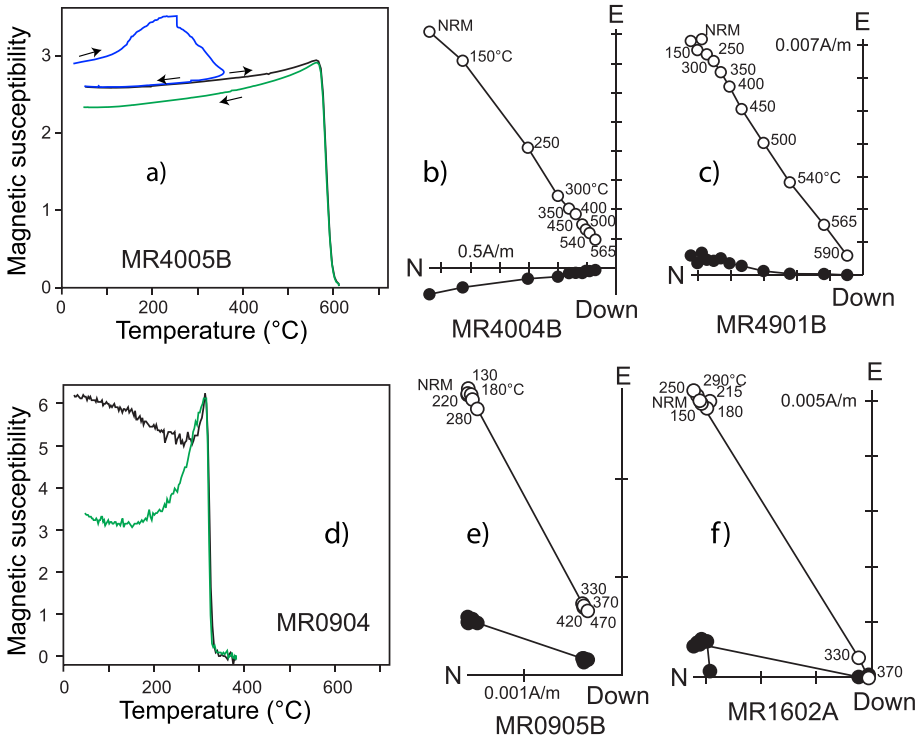

Fig. 7. a) Thermomagnetic experiment for one sample from dike MR40. The first heating curve up to 350 °C and subsequent cooling curve to room temperature are shown in blue. Orthogonal projections (in situ) of thermal demagnetization data of samples from two dikes MR40 (b) and MR49 (c). d) Thermomagnetic experiment for one sample from the IPC country sedimentary rock (site MR09). Orthogonal projections (in situ) of thermal demagnetization data of two samples from the sediment country rock of the IPC ((e) site MR09 and (f) MR16).

Table 1
Site number listed in Table 1; L/P/n: number of vectors, planes ($n = L + P$) used to determine the mean-site characteristic direction defined by its declination, inclination, semi-angle of confidence ($\alpha 95$) and Fisher concentration parameter k. Lat, Lon are latitude and longitude of the virtual geomagnetic pole calculated from the mean-site direction.[2] Tilt corrected characteristic directions for the host rocks.

Site	L/P/n	Dec (IS)	Inc (IS)	α95	k	Lat (VGP)	Lon (VGP)
LC28	5/0/5	52.5	−36.0	8.3	87	41.8	18.4
MR17	7/0/7	40.4	−64.2	3.8	259	55.7	55.9
Gabbros							
MR18	5/0/5	357.0	−55.6	8.3	86	84.7	136.4
MR19	7/0/7	8.5	−47.1	6.5	87	82.0	357.9
MR61	5/0/5	343.6	−54.0	4.1	354	75.9	181.5
MR62	4/0/4	4.5	−54.1	4.1	503	85.0	60.3
MR63	5/0/5	342.9	−55.4	9.0	74	75.1	176.8
LC27	5/0/5	18.2	−55.5	5.2	214	74.2	40.6
MR60	6/0/6	22.7	−58.8	1.7	1624	70.0	48.2
Mean	7	2.3	−55.2	7.2	72		
IPC Salamanca area							
MR65	5/0/5	22.3	−55.8	2.6	888	71.0	39.0
LC16	4/1/5	12.4	−48.7	7.7	115	79.1	11.1
MR58	10/0/10	358.2	−54.7	2.4	403	86.3	133.2
LC23	4/0/4	5.7	−59.0	5.5	279	80.8	80.5
LC24	5/1/6	10.8	−41.8	3.1	510	77.8	343.0
Mean	5	10.0	−52.3	8.2	89		
Tonalite west of Frutillar							
MR02	7/0/7	14.7	−54.9	7.3	70	77.3	37.8
MR06	8/0/8	14.3	−54.5	6.2	80	77.8	35.6
MR22	6/0/6	13.2	−55.6	13.6	25	78.4	42.5
LC07	5/0/5	359.8	−58.5	9.1	72	82.8	110.1
LC08	6/0/6	0.6	−54.5	6.5	107	87.0	99.6
LC10	5/0/5	4.7	−59.5	5.1	223	80.8	85.9
Mean	6	8.1	−56.4	3.7	330		
IPC Frutillar area							
MR27	4/0/4	348.8	−46.1	11.5	65	79.2	222.0
MR30	5/0/5	351.8	−46.6	4.3	324	81.7	228.4
MR32	5/0/5	5.9	−39.7	10.4	55	79.0	319.0
MR33	4/1/5	351.2	−61.1	3.8	470	77.8	141.7
MR34	7/0/7	10.9	−50.1	4.0	234	80.7	13.9
MR46	6/0/6	0.8	−57.3	2.3	828	84.2	102.7
MR47	14/0/14	356.3	−52.2	2.5	250	86.8	187.0
Mean	7	358.2	−50.7	6.7	82		
Mean IPC	25	4.0	−53.7	3.1	90		
Dikes Frutillar area							
MR40	6/0/6	354.9	−55.5	1.6	1858	84.3	155.0
MR41	6/0/6	360.0	−58.4	3.4	396	83.0	108.7
MR42	7/0/7	359.0	−58.8	2.7	485	82.6	115.0
MR43	6/0/6	353.7	−62.3	3.1	474	77.6	130.7
MR44	13/0/13	358.2	−58.2	2.0	442	83.1	120.7
MR48	3/0/3	5.1	−55.8	5.7	467	84.0	65.4
MR49	5/0/5	3.8	−53.8	3.9	383	86.1	53.9
Mean	7	359.4	−57.6	2.7	510		
Mean IPC + Dikes							
Mean D&I	32	3.0	−54.6	2.5	105		
Mean VGP	32			3.0	71	85.7	74.1
Site	**L/P/n**	**Dec**	**Inc**	α95	**k**	Dec^2	Inc^2
Sediments host rocks IPC							
MR04	5/0/5	11.8	−56.0	5.4	200	340.8	−32.0
MR05	5/0/5	10.3	−55.6	7.3	111	289.3	−66.9
MR09	5/0/5	14.8	−59.5	3.4	515	272.4	−21.8
MR16	8/0/8	4.3	−60.2	5.2	114	52.6	−31.0
Volcanic host rocks IPC							
MR07	8/0/8	347.6	−53.8	6.6	72	347.6	−53.8
MR28	7/0/7	21.5	−59.9	3.5	307	351.3	−54.1
MR29	7/0/7	5.1	−49.4	4.7	169	347.1	−40.2
MR55	0/7/7	15.0	−52.1	4.3	349	347.6	−55.3
MR56	7/0/7	341.7	−41.8	4.5	180	326.4	−35.4

(Fig. 8a,b) between the sites suggest a complex magmatic fabric for the gabbro (Table 2).

Despite the scatter (Fig. 8a), the AMS foliation is mainly vertical with an AMS lineation dipping at various angles to the north. For two sites (MR61 and MR62) the AMS is coherent with the AARM fabric (Fig. 8c,d).

5.2. The main tonalitic and granodiorite units

All samples from the Main Tonalitic Unit (MTU) and the Granodioritic Unit (GU) have susceptibility lower than 0.1 SI (Supplementary data and Supplementary Figure 2). All sites, but one, have anisotropy degrees lower than 1.2. The fabric is mainly oblate with a magnetic foliation that is steep in most cases but with varying azimuth (Fig. 9). The magnetic lineations are also highly scattered with a predominant steep dip attitude. At the site level, the magnetic fabric is usually homogeneous as shown by the low ellipses of confidence angles at 95% (Fig. 9, Table 2). When sites are geographically close at the kilometer scale, the magnetic fabrics from nearby sites are also often similar in orientation and shape. An example is shown in Fig. 10 where 4 sites (MR26, MR51, MR53 and MR54) drilled along a 4 km profile have a similar low magnetic fabric ($1.05 < P < 1.07$) and vertical foliation oriented WNW-ESE.

5.3. Comparison of the magnetic fabric of the MME and the host rocks

At five localities we sampled the host rocks and the MME (Fig. 11). In all cases but one, the tensorial mean magnetic fabric of the enclaves is similar to the one from the host rock at the site level but the degree of anisotropy is usually lower with a largest scatter in the direction of minimum and maximum susceptibilities illustrated by larger ellipses of confidence for the enclaves than for the tonalite host rocks.

At site MR06, for which we have more detailed magnetic properties, some samples of the enclaves have more stable remanent magnetization with MDF greater than 20 mT and NRM up to 1 A/m while samples from other enclaves have magnetic characteristics (MDF values and NRM data) similar to those of the tonalite host rocks. A higher content in fine-grained magnetite in some MME could explain the lower anisotropy degree observed.

5.4. The dikes

Samples taken from the mafic dikes have a low degree of anisotropy but well-organized tensors with a sub-vertical magnetic foliation except for site MR48 without significant anisotropy (foliation degree of 1.01). The foliations are almost parallels to the dike orientation. Despite the very low anisotropy, the magnetic lineations are relatively well grouped and dipping to the north (Fig. 12). Flow directions in dikes derived from AMS data are better defined near the chilled margins where elongate and planar particles become imbricated (Tauxe et al., 1998). Unfortunately we have not been able to detect clear imbrication features in these dikes. Epidote veins are oblique to the dike borders but we have not observed this obliquity in the AMS data.

6. Discussion

6.1. Tectonic rotations

The characteristic directions of all sites within the IPC are of normal polarity, in agreement with the radiometric ages and an emplacement during the long normal Cretaceous Superchron. The average characteristic directions obtained for each group of lithologies conforming the IPC are close to those expected for their estimated age of emplacement (90–120 Ma) when compared to the Besse and Courtillot (2002) APWP reference curve or to the mean reference pole proposed by Somoza and Zaffarana (2008). If we exclude the two northern sampled sites (LC28 and MR17), with a clockwise deviated declination, the mean direction determined from 25 IPC sites and 7 mafic dikes is $D = 3.0°$E and $I = -54.6°$N,

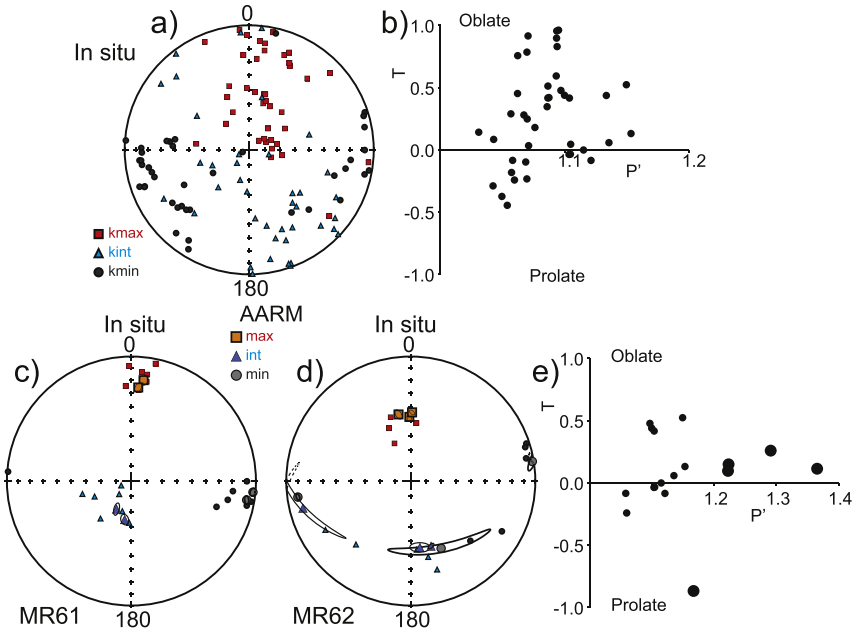

Fig. 8. (a) Stereonet of the principal directions of the AMS ellipsoids samples from the gabbro in in situ coordinate. (b) T-P′ plot for samples of the gabbros. For sites MR61 (c) and MR62 (d) the principal directions of the ARM magnetic fabric are coherent with those of the AMS fabric but with a highest degree of anisotropy. Anisotropy of ARM data are shown with the larges symbols.

($\alpha 95 = 2.5$). If we compare the mean virtual geomagnetic pole (Table 2) with the reference pole calculated by Somoza and Zaffarana (2008) for stable South America (125–90 Ma, Latitude 89.1, Longitude 213.8), there is a clockwise rotation of $4^\circ \pm 3.7$ and a latitudinal displacement of $3.7^\circ \pm 3.1$. This latitudinal displacement is within the resolution of the paleomagnetic method and we will not further speculate about its significance. We however note that the observed inclination for the IPC is in good agreement with the mean inclination observed for the slightly younger Caleu pluton (Parada et al., 2005a) while the mean declination for the Caleu pluton appears rotated 10° clockwise with respect to the mean direction recorded by the IPC. As discussed in more details by Arriagada et al. (2013), there is no significant rotation of the forearc at the latitude of the IPC but there is evidence for clockwise rotation to the south of the studied area including the Caleu pluton. The changing pattern of rotation along the forearc could be related to the subduction of the Juan Fernandez ridge (Arriagada et al., 2013).

6.2. The regional tectonic regime during the IPC emplacement

Despite an about 25 Ma time interval between the emplacement of the different magmatic pulses (Fig. 2), there is no clear apparent polar wander recorded in our paleomagnetic results. This result is in agreement with the mid-Cretaceous polar standstill of South America described by Somoza and Zaffarana (2008) who argue that the beginning of contractional events correlates with the end of this period of slow motion of the South American plate.

This interpretation implies that the emplacement of the IPC occurred during a period of extension rather than within a compressional setting. Except at one locality where we have field evidence for a mylonitic zone (northern part of the IPC), there is no evidence for internal deformation within the IPC. The IPC intrudes sedimentary sequences that are deformed nearby the western edge of the pluton. The tilted limestone record a remagnetization carried by pyrrhotite that is likely associated with contact metamorphism because the in-situ characteristic direction of the limestone is similar to that of the IPC. It is unclear whether the sedimentary layers have been tilted prior or during the emplacement of the IPC which was dated at 99.2 ± 0.6 Ma by U/Pb in titanite in the vicinity of the area (Morata et al., 2006).

At this same latitude but farther west, Arancibia (2004) dated at around 98 Ma (in situ Ar/Ar white-mica) a mylonitic deformation zone related to reverse fault (fault system Silla del Gobernador). This age was interpreted as evidence for compressional regime coeval with exhumation of Paleozoic to Cretaceous units from the Coastal Range (Gana and Zentilli, 2000; Parada et al., 2001; Arancibia, 2004). This observation may indicate that the marine sedimentary sequence was deformed during the emplacement of the *c.a.* 100 Ma MTU. The extensional structures of "Lo Prado basin" could have accommodated the magma emplacement and explain the deformation style observed in the sedimentary sequence (an east vergence overturned anticline), by the inversion of these extensional structures. Thus, the "Lo Prado basin" tectonic inversion would be contemporary with the compressional tectonic regime proposed by Arancibia (2004).

6.3. Intrusive strain and emplacement mode

Magnetite is the main magnetic carrier of the susceptibility at all sites. The degree of anisotropy is lower than 1.2 except at site LC26 that is the only site where there is evidence for ductile deformation.

For the layered gabbros with high magnetic susceptibility, the anisotropy is not very strong and well-defined ellipsoids are observed for only two sites.

The magnetic fabric detected in the MME is coaxial with the magnetic fabric of the host tonalite unit. This observation indicates that the magnetic fabric in the MME is related to the same strain affecting the host rock during the late stage of emplacement. This suggests that the MME had probably the same viscosity than the tonalite. The same observation has been made in previous AMS studies of MME rich plutons (Hrouda et al., 1999).

At a regional scale there is a significant variation in the orientation of the AMS ellipsoids (Fig. 13) and this raises doubts about the existence of a regional compressive tectonic stress during the

Table 2
N: number of specimens used to calculate the mean tensor. D,I, P1 and P1 are the declination, inclination, angles of the ellipse of confidence for the direction of the maximum (K_{max}) and minimum (K_{min}) axes of the mean-site ellipsoid. Lin: degree of lineation; Fol: degree of foliation; P & P′ are the degree of anisotropy and corrected anisotropy respectively according to Jelinek (1978). *T* parameter defining the type of ellipsoid with $T = 1$ for a pure oblate and $T = -1$ for a pure prolate ellipsoid.

		K_{max}				K_{min}								
Site	N	D	I	P1	P2	D	I	P1	P2	Lin	Fol	P	P′	T
Gabbro														
MR18	3	345.3	77.8	58.8	28.8	122.8	9.1	80.0	15.3	1.043	1.097	1.140	1.148	0.37
MR19	10	21.7	52.0	24.4	6.4	259.0	22.9	20.6	9.7	1.017	1.041	1.058	1.060	0.40
MR61	7	5.1	17.2	10.1	5.7	98.4	10.5	14.4	5.7	1.054	1.062	1.117	1.120	0.07
MR62	5	344.2	53.2	12.5	10.6	82.2	5.9	31.6	4.8	1.033	1.038	1.072	1.073	0.07
Other intrusive rocks														
LC07	10	95.0	4.8	31.8	2.9	3.9	11.8	6.7	2.9	1.025	1.109	1.134	1.145	0.61
LC08	10	109.0	72.1	19.7	6.6	355.6	7.3	25.2	7.6	1.037	1.104	1.141	1.150	0.47
LC09	10	187.0	43.4	15.5	11.3	56.4	34.5	16.5	5.3	1.069	1.044	1.113	1.117	−0.22
LC10	9	352.5	3.9	17.0	9.9	84.0	21.9	38.4	13.8	1.044	1.037	1.081	1.083	−0.08
LC15	5	151.1	20.7	32.3	16.6	270.6	52.6	63.3	11.7	1.015	1.006	1.021	1.022	−0.45
LC16	6	263.5	62.5	56.1	14.9	163.5	5.1	46.2	17.5	1.005	1.012	1.017	1.018	0.39
LC17	8	5.8	18.5	44.6	7.8	245.7	56.3	8.9	4.8	1.006	1.033	1.039	1.042	0.68
LC18	13	354.1	2.2	13.7	2.5	259.4	64.7	4.1	2.4	1.012	1.048	1.059	1.063	0.59
LC23	10	293.5	61.5	53.2	3.8	166.4	18.1	6.9	2.7	1.003	1.048	1.051	1.057	0.89
LC24	9	69.1	71.5	24.0	11.5	282.8	15.6	21.6	16.6	1.006	1.006	1.012	1.012	0.05
LC25	12	53.8	54.5	13.3	3.3	202.0	31.2	8.5	3.4	1.035	1.076	1.111	1.116	0.36
LC26	9	206.9	12.9	16.6	3.7	113.1	16.4	6.8	3.7	1.041	1.359	1.400	1.462	0.77
LC27	5	272.4	69.3	28.8	13.9	147.9	12.1	33.8	7.1	1.077	1.106	1.183	1.192	0.15
LC28	11	30.5	76.6	21.4	5.2	137.7	4.0	11.0	5.2	1.028	1.037	1.066	1.067	0.13
MRE1	12	118.8	41.7	15.1	6.5	19.6	10.2	27.4	5.0	1.030	1.026	1.056	1.057	−0.06
MR01	9	117.5	43.4	25.5	9.3	23.6	4.0	21.7	10.8	1.050	1.044	1.094	1.096	−0.07
MR02	11	157.5	50.7	26.3	12.5	271.4	18.3	35.0	12.3	1.019	1.017	1.036	1.036	−0.04
MR03	8	157.5	59.2	22.0	7.5	33.2	18.6	14.1	7.2	1.030	1.026	1.056	1.057	−0.06
MRE6	9	76.8	34.4	40.4	9.7	170.9	5.9	17.6	9.6	1.007	1.029	1.036	1.038	0.60
MR06	6	279.9	71.6	60.7	12.9	177.7	4.0	26.9	4.6	1.006	1.029	1.035	1.038	0.64
MR08	9	25.8	56.6	13.9	2.4	282.3	8.8	4.4	2.9	1.020	1.109	1.128	1.141	0.68
MR10	6	194.4	58.7	27.9	4.1	92.7	7.1	8.4	4.5	1.039	1.066	1.105	1.108	0.25
MR11	9	185.5	15.1	24.0	17.0	81.5	41.9	60.6	16.6	1.023	1.007	1.031	1.032	−0.52
MR12	8	176.3	55.8	9.6	5.7	57.2	18.3	21.4	6.0	1.036	1.036	1.072	1.074	0.00
MR13	7	199.3	65.9	21.2	5.8	34.4	23.4	8.0	4.0	1.030	1.093	1.123	1.131	0.50
MR14	8	190.2	53.1	14.9	3.5	62.7	24.6	9.8	2.6	1.033	1.064	1.098	1.101	0.31
MR17	9	256.8	69.9	7.5	3.7	346.8	0.0	52.3	3.5	1.015	1.001	1.016	1.018	−0.85
MRE20	11	231.5	26.6	66.3	13.4	330.9	18.2	19.9	7.4	1.002	1.018	1.020	1.022	0.77
MR21	8	217.9	19.3	27.8	11.3	308.6	1.9	29.6	16.1	1.029	1.030	1.060	1.061	0.01
MR22	12	160.2	31.7	38.7	14.5	28.9	46.9	65.1	15.6	1.008	1.002	1.010	1.011	−0.54
MR23	10	132.0	41.6	11.4	5.1	19.6	23.2	25.9	8.2	1.056	1.033	1.088	1.091	−0.26
MR23	8	127.8	38.7	9.9	3.9	24.6	15.8	18.7	8.2	1.055	1.042	1.097	1.100	−0.13
MRE24	9	132.7	30.2	33.7	20.0	41.2	2.7	31.3	12.1	1.018	1.024	1.042	1.043	0.14
MR25	9	96.5	51.5	15.6	9.6	212.5	19.2	23.3	13.3	1.029	1.025	1.054	1.055	−0.07
MR26	7	301.0	14.7	43.0	3.9	31.7	2.4	9.2	3.8	1.007	1.057	1.064	1.071	0.77
MR27	5	340.6	36.5	23.3	16.4	118.4	45.0	44.7	17.8	1.004	1.004	1.007	1.008	−0.01
MR30	5	126.4	65.2	57.8	29.6	225.9	4.4	63.4	30.1	1.009	1.008	1.017	1.017	−0.09
MR31	5	337.0	61.9	30.9	1.2	199.8	21.4	6.8	1.6	1.033	1.043	1.076	1.078	0.13
MR32	5	184.0	8.8	29.3	26.2	295.2	66.9	53.2	19.2	1.006	1.003	1.009	1.009	−0.35
MR33	7	270.6	57.9	44.2	21.2	172.2	5.2	82.6	21.1	1.008	1.004	1.012	1.012	−0.34
MR34	8	221.1	0.9	4.3	2.6	130.3	40.6	9.6	2.8	1.021	1.048	1.069	1.071	0.38
MR35	6	241.6	37.7	16.8	11.6	337.5	7.6	20.3	11.6	1.009	1.009	1.017	1.018	−0.01
MR36	9	2.1	26.4	21.5	8.3	237.2	49.0	9.7	3.6	1.010	1.028	1.038	1.039	0.47
MR37	8	147.6	64.0	24.5	7.7	25.4	14.6	16.6	9.4	1.035	1.092	1.127	1.135	0.44
MR38	11	125.2	61.0	17.4	7.5	242.0	14.0	19.1	7.8	1.059	1.027	1.086	1.090	−0.37
MR39	6	251.3	73.2	47.1	7.1	158.9	0.7	9.4	3.9	1.020	1.142	1.162	1.180	0.75
MR45	9	304.8	48.5	62.2	8.5	53.5	15.9	17.3	9.5	1.001	1.007	1.008	1.009	0.79
MR46	10	220.7	15.9	36.5	22.3	26.7	73.6	22.3	16.9	1.002	1.003	1.005	1.005	0.17
MR50	13	197.6	16.6	31.1	9.1	102.8	15.7	9.5	8.9	1.020	1.068	1.088	1.094	0.54
MR51	14	326.3	25.1	73.4	7.5	231.5	10.2	13.1	8.8	1.003	1.050	1.054	1.060	0.88
MR53	5	317.7	61.1	21.8	12.5	208.6	10.2	26.5	11.7	1.023	1.042	1.065	1.067	0.29
MR54	11	112.0	21.0	45.0	7.6	20.9	2.9	8.2	7.7	1.009	1.049	1.057	1.062	0.69
MR47	13	19.3	3.3	10.2	6.8	110.1	13.3	10.9	4.9	1.025	1.032	1.057	1.058	0.12
MR57	13	176.0	3.5	26.4	8.0	267.0	16.0	11.7	6.6	1.027	1.064	1.091	1.096	0.40
MR58	10	23.2	19.6	33.3	3.5	196.7	70.3	4.2	3.6	1.007	1.047	1.053	1.059	0.75
MR65	7	10.9	45.0	28.3	13.6	158.2	40.1	40.6	15.8	1.017	1.022	1.039	1.039	0.15
Dikes Frutillar														
MR40	16	14.9	48.1	13.3	7.8	271.1	12.1	8.0	4.8	1.004	1.018	1.022	1.024	0.64
MR41	17	335.2	51.8	16.7	7.7	94.3	21.0	12.2	5.0	1.003	1.016	1.020	1.021	0.65
MR42	15	192.4	81.4	60.3	10.6	70.0	4.6	13.1	7.2	1.000	1.012	1.012	1.014	0.92
MR43	14	340.1	45.8	40.2	11.7	72.3	2.1	18.6	12.1	1.002	1.014	1.016	1.017	0.71
MR44	12	163.8	28.0	58.5	9.5	66.9	12.8	16.2	5.7	1.002	1.012	1.014	1.015	0.68
MR48	10	264.8	36.7	24.6	21.8	174.8	0.0	55.8	20.3	1.001	1.001	1.002	1.002	−0.33
MR49	9	337.8	25.8	33.3	12.1	70.3	5.2	21.6	10.0	1.001	1.002	1.003	1.003	0.33

Table 2 (*continued*)

		K_{max}				K_{min}								
Site	N	D	I	P1	P2	D	I	P1	P2	Lin	Fol	P	P′	T
Volcanic rocks														
MR28	6	156.0	37.0	54.4	29.9	47.0	23.3	56.0	29.2	1.007	1.005	1.013	1.013	−0.13
MR29	8	81.7	6.9	14.2	11.2	266.5	83.1	31.9	11.4	1.008	1.027	1.035	1.037	0.52
MR55	12	87.2	18.9	33.4	9.8	252.7	70.5	22.9	8.6	1.004	1.006	1.010	1.010	0.14

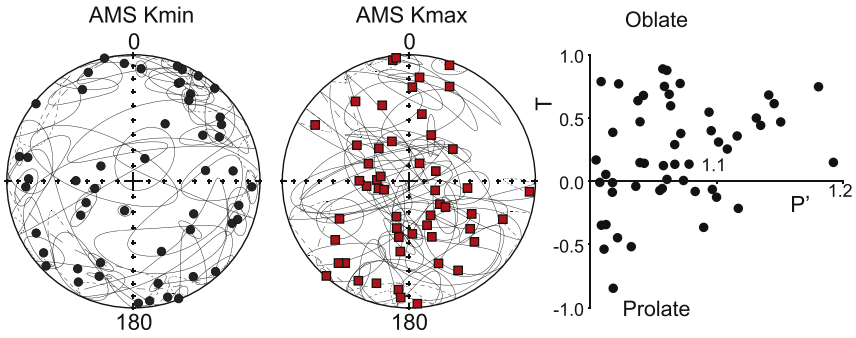

Fig. 9. Stereonets of the poles of the magnetic foliations observed in the IPC (left) and the down-dip direction of the magnetic lineation (center). (right) T-P′ plot of the magnetic fabric. Only one site (LC46) with a corrected anisotropy degree P′ > 1.2 is not shown on this graph.

emplacement. The same observation can be found in the AMS study of the Caleu pluton located less than 100 km to the south of the IPC (Parada et al., 2005b). For this pluton, changes in the orientation of the magnetic fabrics appear strongly related to the shape of its borders and roof. However, in map view, this pluton does not present a preferential orientation of its border. In contrast, the IPC plutonic units seem to correspond to large N–S oriented bodies (Fig. 13). Thus we should expect that the magnetic fabric in the IPC should also be biased toward a preferential N–S orientation. This is not the case and the nearly E-W magnetic foliation observed at some sites could indicate that the IPC is not constituted by large N–S oriented magmatic bodies but by several closely spaced amalgamated nearby plutons aligned along the N–S oriented Cretaceous arc. This interpretation is also supported by the distribution of the ages. The oldest ages are found in the mafic unit (MU) located in the northern part and western border of the IPC. However, the Trondhjemitic Unit (TU), outcropping north of Caimanes village (Figs. 1 and 13) and dated at 110 Ma, appear as discrete pulses along the IPC, meanwhile the Main Tonalitic Unit, with an age of about 100 Ma, seems to be disposed along a NS band. The expected eastward younging age progression is rebutted by the two biotite $^{40}Ar/^{39}Ar$ ages of ~107–108 Ma obtained in granodiorite rock in which intruded the Frutillar mafic dikes (see Figs. 1 and 2).

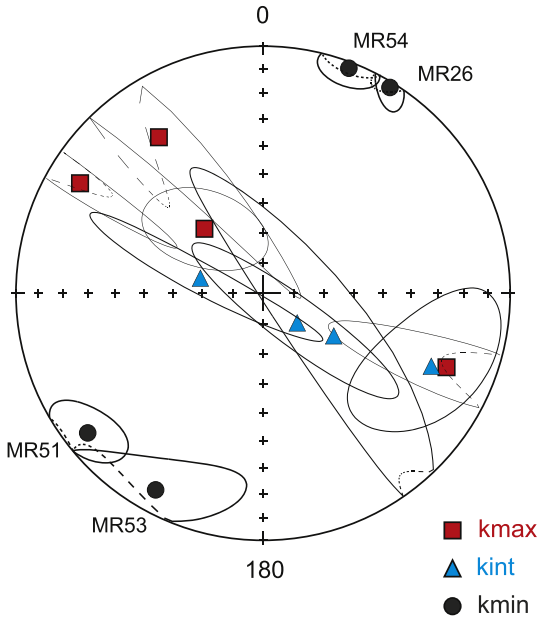

Fig. 10. Stereonet of the principal directions of the AMS ellipsoids for 4 nearby sites MR26, MR51, MR53, MR54 showing that the magnetic fabric is coherent within sites a few kilometers apart.

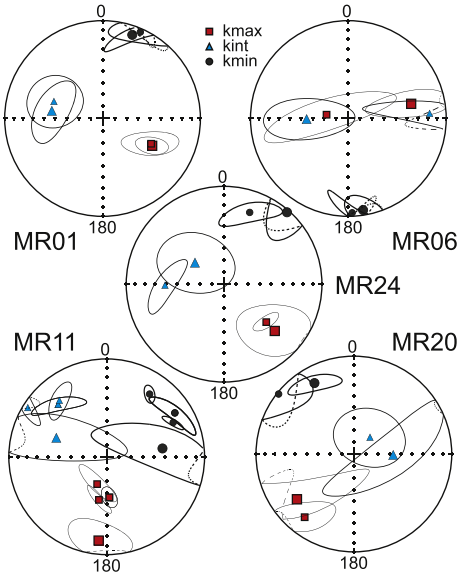

Fig. 11. Comparison of the principal directions of the AMS ellipsoids in the enclaves and the host intrusive rocks at five sites. The AMS in the enclaves is similar to the one in the host rock except at site MR11 where the magnetic fabric is statistically different from the fabric in sites from nearby intrusive rocks (MR12, MR13 and MR14). Mean tensors calculated from several samples in different enclaves are shown with large symbols while the results in the intrusive host rocks are shown with smallest size symbols.

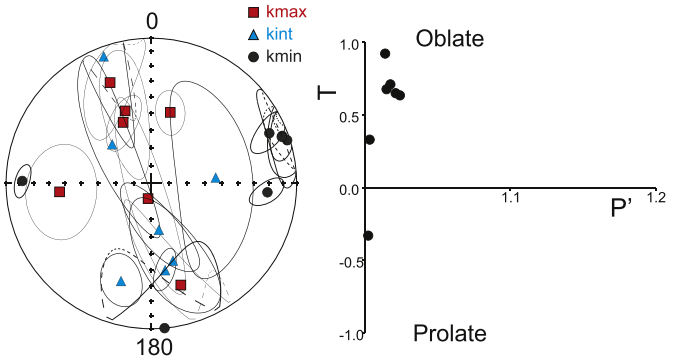

Fig. 12. (left) Stereonet of the principal directions of the AMS ellipsoids in the dikes. (right) T-P′ plot for the site-mean tensor. The two dikes (MR48 and MR49) have a very low anisotropy while an oblate magnetic foliation is recorded in the other dikes.

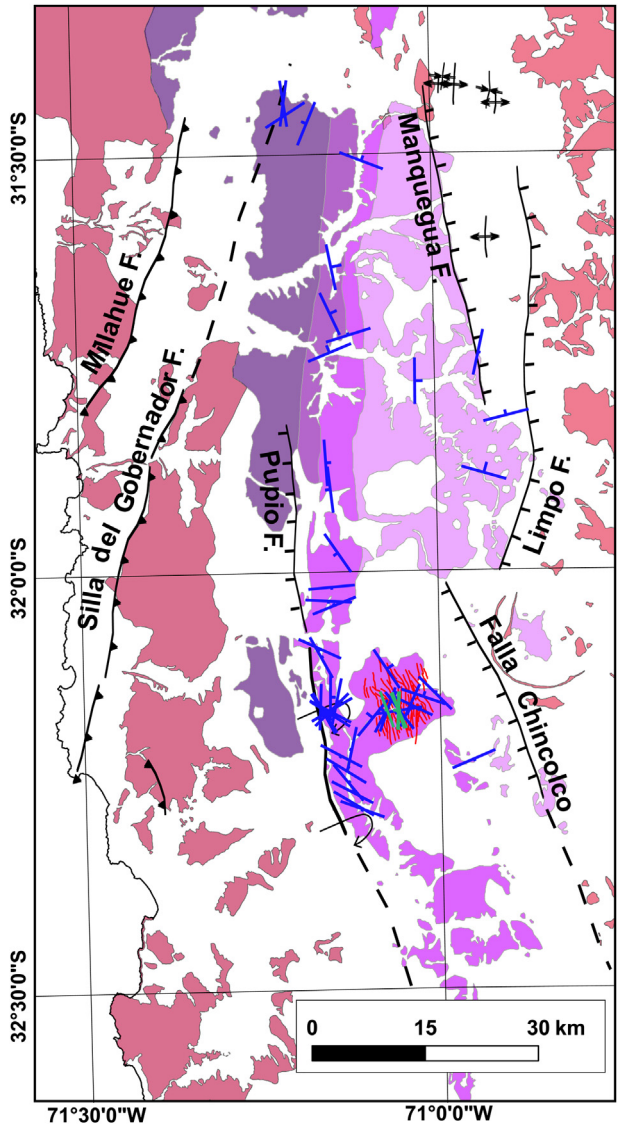

Fig. 13. Map of the magnetic foliation across the IPC. The dip of the foliation plane is shown by the length of the bar with shortest bars corresponding to steeply dipping magnetic foliations (see Figs. 1 and 2 for more geological information).

6.4. The mafic enclaves and dikes

The MME are distributed heterogeneously in the MTU, mainly at isolated central zones and borders of the southern part of this magmatic pulse. The MME are generally rounded to sub-rounded, fine grain size and ellipsoidal shapes. Their color varies according to composition, being the black and gray MME diorites and monzodiorites while MME with lighter color are quartz diorites and quartz monzodiorites.

The mineralogy, textures, observed morphological characteristics and P-T conditions estimations in the MME, indicate the MTU unit with MME was generated by two interacting felsic and mafic magmas (Varas et al., 2009, 2012). This interpretation is also confirmed by the similitude in ages obtained in biotite from MME (sample MR01, 101.2 ± 0.1 Ma) and hosting tonalite (sample MR08, 100.8 ± 0.1 Ma, sample MR39, 98.2 ± 0.1 Ma). Moreover, these Ar/Ar ages are consistent with U/Pb ages obtained in titanite from the MTU, suggesting high cooling rate after emplacement. We suggest that the mafic magma from which MME formed would ascend through dike-shaped feeders.

The two new biotite $^{40}Ar/^{39}Ar$ ages obtained in the plutonic unit intruded by the dike complex in Quebrada Frutillar are significantly older (107–108 Ma) than the MTU (≈100 Ma). According to these new ages, and the similitude in magnetic properties, we propose that these granodiorites belong to the TU and the mafic dikes from *Quebrada Frutillar* and the mafic enclaves observed in the MTU could be then contemporaneous and generated from the same mafic magma reservoir.

There is no elevation difference between the *Quebrada Frutillar* area with the dike swarm and the MTU. The paleomagnetic study of the dike swarm indicates titanomagnetite slightly altered to titanomaghemite as the magnetic carrier in the dike. This suggests that the dikes intruded a relatively cold intrusive.

Moreover the low degree of AMS recorded by the dikes also suggests low strain and rapid cooling, a case very different from the one described for the Concon dyke swarm by Creixell et al. (2006). This interpretation is in agreement with petrologic data of the MME and the tonalite indicating that the tonalite unit was emplaced at shallow crustal level.

Finally, the coincidence between U/Pb ages and the new Ar/Ar ages obtained in this work indicate high cooling rate for the MTU. Moreover, because biotite closure temperature for Ar/Ar system is close to 350 °C, the biotite plateau ages obtained in rocks belonging to the TU and MTU suggest that after emplacement and cooling of the IPC, this complex does not evidence any low- to medium-temperature event that could reset the primary magmatic ages. Consequently, all the magnetic properties observed in the IPC and presented in this work are related to primary magmatic processes (magmatic emplacement) and not in relation with any post-magmatic event that could reset the primary magnetic foliation.

7. Conclusions

Paleomagnetic results were obtained in rocks of the IPC as well as in the host sedimentary rock. The characteristic directions of all sites within the IPC are of normal polarity, in agreement with the radiometric ages and an emplacement during the long normal Cretaceous Superchron. A very low value of 4° ± 3.7° clockwise rotation is obtained for the area of the Chilean forearc between 31°30'S and 32°30'S.

AMS results from the different lithological units of the Illapel Plutonic Complex are interpreted as primary magmatic fabrics acquired during the late stages of pluton emplacement. Our samples are not homogeneously distributed within the different magmatic pulses but still show some similar characteristics: a) the degree of

anisotropy is lower than 1.2 except at one site where there is evidence for ductile deformation; b) at a regional scale there is a significant variation in the orientation of the AMS ellipsoids. These elements, together with the very homogeneous characteristic directions of all sites, make us question the existence of a regional compressive tectonic stress during the emplacement of the IPC.

The paleomagnetic study of the IPC supports the mid-Cretaceous polar standstill of South America (Somoza and Zaffarana, 2008). Magnetic fabrics are best interpreted as evidence of magmatic origin with the emplacement of the IPC occurring prior to the beginning of compressive deformation in the Andes of Central Chile.

Acknowledgments

We are indebted to Project Fondecyt 1080468: "The anatomy, nature, ascent and emplacement of the Illapel Plutonic Complex, Coastal Range, Central Chile", and to the IRD for the logistical support during field work (especially to Sergio Villagrán). Finally, we gratefully acknowledge the "Departamento de Postgrado y Postítulo de la Vicerrectoría de Asuntos Académicos de la Universidad de Chile" and its program "Becas de Estadías Cortas de investigación". We thank Christian Creixell for his comments on an early version of this manuscript. We acknowledge Andres Folguera and an anonymous referee for their comments and suggestions to improve the manuscript. This work is a contribution to the Fondap-Conicyt Project 15090013.

Appendix A. Supplementary data

Supplementary data related to this article can be found at http://dx.doi.org/10.1016/j.jsames.2013.11.007.

References

Aguirre, L., Levi, B., Nyström, J.O., 1989. The link between metamorphism, volcanism and geotectonic setting during the evolution of the Andes. In: Daly, B.W.D., Cliff, R.A., Yardley, J.S. (Eds.), Evolution of Metamorphic Belts 43. Geological Society of London, pp. 223–232. Special Publication.

Aguirre, L., Féraud, G., Morata, D., Vergara, M., Robinson, D., 1999. Time interval between volcanism and burial metamorphism and rate of basin subsidence in a Cretaceous Andean extensional setting. Tectonophysics 313, 433–447.

Arancibia, G., 2004. Mid-Cretaceous crustal shortening: evidence from a regional-scale ductile shear zone in the Coastal Range of central Chile (32° S). J. South Am. Earth Sci. 17, 209–226.

Arriagada, C., Ferrando, R., Córdova, L., Morata, D., Roperch, P., 2013. The Maipo Orocline: a first scale structural feature in the Miocene to Recent geodynamic evolution in the central Chilean Andes. Andean Geol. 40 (3), 419–437.

Astudillo, N., Roperch, P., Townley, B., Arriagada, C., 2005. A Paleomagnetic Study of the Chuquicamata Porphyry Copper Deposits, Northern Chile. IAGA Assembly, Toulouse Francia.

Besse, J., Courtillot, V., 2002. Apparent and true polar wander and the geometry of geomagnetic field in the last 200 million years. J. Geophys. Res. 107, 2300.

Boric, R., Munizaga, F., 1994. Geocronología Ar–Ar y Rb–Sr del depósito estratoligado de cobre El Soldado (Chile central), vol. 45. Comunicaciones-Universidad de Chile, pp. 135–148.

Borradaile, G.J., Henry, B., 1997. Tectonic applications of mag-netic susceptibility and its anisotropy. Earth Sci. Rev. 42, 49–93.

Cobbold, P.R., Rossello, E., Roperch, P., Arriagada, C., Gómez, L., Lima, C., 2007. Distribution, timing, and causes of Andean deformation across South America 272. Geological Society, London, pp. 321–343. Special Publications.

Creixell, C., Parada, M.A., Roperch, P., Morata, D., Arriagada, C., Pérez de Arce, C., 2006. Syntectonic emplacement of the Concon mafic dike swarm, Coastal Range, central Chile (33°S). Tectonophysics 425, 101–122.

Dekkers, M.J., Mattri, J.L., Fillion, G., Rochette, P., 1989. Grain-size dependence of the magnetic behavior of pyrrhotite during its low temperature transition at 34 K. Geophys. Res. Lett. 16, 855–858.

Feinberg, J.M., Scott, G.R., Renne, P.R., Wenk, H.R., 2005. Exsolved magnetite inclusions in silicates: features determining their remanence behavior. Geology 33, 513–516.

Fuentes, F., Féraud, G., Aguirre, L., Morata, D., 2005. $^{40}Ar/^{39}Ar$ dating of volcanism and subsequent very low-grade metamorphism in a subsiding basin: example of the Cretaceous lava series from central Chile. Chem. Geol. 214, 157–177.

Gana, P., Zentilli, M., 2000. Historia termal y exhumación de intrusivos de la Cordillera de la Costa de Chile central. In: Congreso Geológico Chileno, No. 9, Actas, vol. 2, pp. 664–668 (Puerto Varas).

Godoy, E., Rayner, N., Davis, B., 2006. Edad U-Pb cretácica temprana de ignimbritas y andesitas en la Depresión Central, VI Región, Chile: implicancias geotectónicas. In: XI Congreso Geológico Chileno, Actas, vol. 1, pp. 229–232.

Hrouda, F., Taborska, S., Schulmann, K., Jezek, J., Dolejs, D., 1999. Magnetic fabric and rheology of co-mingled magmas in the Nasavrky Plutonic Complex (E Bohemia): implications for intrusive strain regime and emplacement mechanism. Tectonophysics 307, 93–111.

Jelinek, V., 1978. Statistical processing of anisotropy of magnetic susceptibility measured on groups of specimens. Studia Geoph. Geod. 22, 50–62.

Levi, B., 1969. Burial metamorphism of a Cretaceous volcanic sequence west from Santiago, Chile. Contrib. Mineral. Petrol. 24, 30–49.

Levi, B., Aguirre, L., Nyström, J.O., 1982. Metamorphic gradients in burial metamorphosed vesicular lavas: comparison of basalt and spilite in Cretaceous basic flows from central Chile. Contrib. Mineral. Petrol. 80, 49–58.

Levi, B., Aguirre, L., Nyström, J.O., Padilla, H., Vergara, M., 1989. Low-grade regional metamorphism in the Mesozoic-Cenozoic volcanic sequences of the Central Andes. J. Metamorph. Geol. 7, 487–495.

Martínez-Pardo, R., Gallego, A., Martínez-Guzmán, R., 1994. Middle Albian marine planktonic microfossils from the Santiago basin, central Chile: their depositional and paleogeographic meaning. Revista Geológica de Chile 21, 173–187.

Mpodozis, C., Ramos, V., 1989. The Andes of Chile and Argentina. In: Ericksen, G., Cañas-Pinochet, M., Reinemund, J. (Eds.), Geology of the Andes and its Relation to Hidrocarbon and Mineral Resources, Circum-Pacific Council for Energy and Mineral Resources, Earth Sciences Series, vol. 11, pp. 59–90.

Morata, D., Aguirre, L., Féraud, G., Fuentes, F., Parada, M.A., Vergara, M., 2001. The Lower Cretaceous volcanism in the Coastal Range of central Chile: geochronology and isotopic geochemistry. In: South American Symposium on Isotope Geology No. 3Sociedad Geológica de Chile, pp. 321–324. ExtendedAbstracts Volume (CD).

Morata, D., Aguirre, L., 2003. Extensional Lower Cretaceous volcanism in the Coastal Range of central Chile: geochemistry and petrogenesis. J. South Am. Earth Sci. 16, 459–476.

Morata, D., Féraud, G., Schärer, U., Aguirre, L., Belmar, M., Cosca, M., 2006. A new geochronological framework for Lower Cretaceous magmatism in the Coastal Range of central Chile. In: Congreso Geológico Chileno, No. 11, Actas, vol. 2, pp. 509–512 (Antofagasta).

Morata, D., Varas, M.I., Higgins, M., Valencia, V., Verhoort, J., 2010. Episodic emplacement of the Illapel Plutonic Complex (Coastal Cordillera, central Chile): Sr and Nd isotopic, and zircon U-Pb geochronological constraints. In: South American Symposium on Isotope Geology, No. 7. Brasilia (Brasil).

Muñoz Cristi, J., 1942. Rasgos generales de la constitución geológica de la Cordillera de la Costa, especialmente en la Provincia de Coquimbo. In: Congreso Panamericano de Ingeniería de Minas y Geología, No. 1, Anales, vol. 2, pp. 285–318. Santiago (Chile).

Nasi, C., Thiele, R., 1982. Estratigrafía del Jurásico y Cretácico de la Cordillera de la Costa al sur del río Maipo entre Melipilla y Laguna de Aculeo (Chile Central). Revista Geológica de Chile 16, 81–99.

Parada, M.A., Rivano, S., Sepúlveda, P., Hervé, M., Hervé, F., Puig, A., Munizaga, F., Brook, M., Pankhurst, R., Snelling, N., 1988. Mesozoic and Cenozoic plutonic development in the Andes of central Chile (30°30' - 32°30'S). J. South Am. Earth Sci. 1, 249–260.

Parada, M.A., Nyström, J.O., Levi, B., 1999. Multiple sources for the Coastal Batholith of central Chile (31–34°S): geochemical and Sr–Nd isotopic evidence and tectonic implications. Lithos 46, 505–521.

Parada, M.A., Féraud, G., Aguirre, L., Fuentes, F., Morata, D., Vergara, M., Larrondo, P., Palacios, C., 2001. U-Pb, $^{40}Ar–^{39}Ar$ and fission-track geochronology of the Early Cretaceous Caleu pluton and its volcanic envelope, Coastal Range of central Chile: Tectonic and metamorphic implications. In: Symposium on Isotope Geology, No. 3, pp. 612–615. Abstracts, Pucón (Chile).

Parada, M.A., Larrondo, P., Guiresse, C., Roperch, P., 2002. Magmatic gradients in the Cretaceous Caleu pluton (central Chile): injections of pulses from a stratified magma reservoir. Gondwana Res. 5, 307–324.

Parada, M.A., Féraud, G., Fuentes, F., Aguirre, L., Morata, D., Larrondo, P., 2005a. Ages and cooling history of the Early Cretaceous Caleu pluton: testimony of a switch from a rifted to a compressional continental margin in central Chile. J. Geol. Soc. London 162, 273–287.

Parada, M.A., Roperch, P., Gírese, C., Ramírez, E., 2005b. Magnetic fabrics and compositional evidence for the construction of the Caleu pluton by multiple injections, Coastal Range of central Chile. Tectonophysics 399, 399–420.

Ramos, V., Aleman, A., 2000. Tectonic evolution of the Andes. In: Cordani, U., Milani, E.J., Thomaz Filho, A., Campos, D.A. (Eds.), Tectonic Evolution of South America, pp. 635–685, 31st International Geological Congress, Rio de Janeiro. Publisher, Town.

Renne, P.R., Swisher, C.C., Deino, A.L., Karner, D.B., Owens, T.L., DePaolo, D.J., 1998. Intercalibration of standards, absolute ages and uncertainties in $^{40}Ar/^{39}Ar$ dating. Chem. Geol. 145, 117–152.

Rivano, S., Sepúlveda, P., Hervé, M., Puig, A., 1985. Cronología K-Ar de las rocas intrusivas entre los 31°-32°S, latitud sur, Chile. Revista Geológica de Chile 24, 63–74.

Rivano, S., Sepúlveda, P., 1991. Hoja Illapel, Región de Coquimbo. Servicio Nacional de Geología y Minería. Carta Geológica de Chile No. 69 (escala 1:250.000). Santiago.

Rivano, S., Sepúlveda, P., Boric, R., Espiñeira, D., 1993. Hojas Quillota y Portillo, V Región. Servicio Nacional de Geología y Minería. Carta Geológica de Chile No. 73 (escala 1: 250.000). Santiago.

Robinson, D., Bevins, R.E., 1989. Diastathermal (extensional) metamorphism at very low grades and possible high grade analogues. Earth Planet. Sci. Lett. 92, 81–88.

Ruffet, G., Féraud, G., Amouric, M., 1991. Comparison of $^{40}Ar/^{39}Ar$ conventional and laser dating of biotites from the North Tregor batholiths. Geochim. Cosmochim. Acta 55, 1675–1688.

Ruffet, G., Féraud, G., Balèvre, M., Kiénast, J.-R., 1995. Plateau ages and excess argon in phengites: an ^{40}Ar-^{39}Ar laser probe study of Alpine micas (Sesia Zone, Western Alps, northern Italy). Chem. Geol. 121, 327–343 (Isotopic Geoscience Section).

Ruffet, G., Gruau, G., Ballèvre, M., Féraud, G., Philippot, P., 1997. Rb-Sr and ^{40}Ar-^{39}Ar laser probe dating of high-pressure phengites from the Sesia zone (western Alps): underscoring of excess argon and new age constraints on the high-pressure metamorphism. Chem. Geol. 141, 1–18.

Somoza, R., Zaffarana, C.B., 2008. Mid-Cretaceous polar standstill of South America, motion of the Atlantic hotsposts and the birth of the Andean Cordillera. Earth Planet. Sci. Lett. 271, 267–277.

Tauxe, L., Gee, J.S., Staudigel, H., 1998. Flow directions in dikes from anisotropy of magnetic susceptibility data: the bootstrap way. J. Geophys. Res. 103, 17775–17790.

Thomas, H., 1958. Geología de la Cordillera de la Costa entre el Valle de La Ligua y la Cuesta Barriga. Instituto de Investigaciones Geológicas, p. 86. Boletín, No. 2, (Santiago).

Tunik, M., Folguera, A., Naipauer, M., Pimentel, M., Ramos, V.A., 2010. Early uplift and orogenic deformation in the Neuquén basin: constraints on the Andean uplift from U/Pb and Hf analyses of detrital zircons. Tectonophysics 489, 258–273.

Varas, M.I., Morata, D., Arriagada, C., Ferrando, R., Higgins, M., 2009. Distribución y características morfológicas de los enclaves máficos del borde sur del Complejo Plutónico Illapel (CPI). In: Congreso Geológico Chileno, No. 12. Santiago (Chile).

Varas, M.I., Morata, D., Higgins, M., 2012. P-T conditions of crystallization of mafia microgranular enclaves from the Illapel Plutonic Complex (IPC). In: Congreso Geológico Chileno, No 12. Antofagasta (Chile).

Vergara, M., Drake, R., 1979. Edades K/Ar en secuencias volcánicas continentales postneocomianas de Chile Central; su depositación en cuencas intermontanas restringidas. Revista de la Asociación Geológica Argentina 34, 42–52.

Vergara, M., Levi, B., Nyström, J., Cancino, A., 1995. Jurassic and Early Cretaceous island arc volcanism, extension and subsidence in the Coast Range of central Chile. Geol. Soc. Am. Bull. 107, 1427–1440.

Wall, R., Sellés, D., Gana, P., 1999. Área Tiltil-Santiago, Región Metropolitana. Servicio Nacional de Geología y Minería, Santiago. Mapas Geológicos, N°11, escala 1:100.000.